# High-order harmonic generation by chirped and self-guided femtosecond laser pulses. II. Time-frequency analysis

V. Tosa,[1,2] H. T. Kim,[1] I. J. Kim,[1] and C. H. Nam[1]
[1]*Department of Physics, KAIST, Yuseong-gu, Daejeon, 305-701 Korea*
[2]*National Institute for R&D of Isotopic and Molecular Technologies, Cluj-Napoca, Romania*
(Received 7 December 2004; published 16 June 2005)

We present a time-dependent analysis of high-order harmonics generated by a self-guided femtosecond laser pulse propagating through a long gas jet. A three-dimensional model is used to calculate the harmonic fields generated by laser pulses, which only differ by the sign of their initial chirp. The time-frequency distributions of the single-atom dipole and harmonic field reveal the dynamics of harmonic generation in the cutoff. A time-dependent phase-matching calculation was performed, taking into account the self-phase modulation of the laser field. Good phase matching holds for only few optical cycles, being dependent on the electron trajectory. When the cutoff trajectory is phase matched, emitted harmonics are locked in phase and the emission intensity is maximized.

DOI: 10.1103/PhysRevA.71.063808 PACS number(s): 42.65.Ky, 32.80.Rm, 52.38.Hb

## I. INTRODUCTION

High-order harmonics (HH) generation is one of the most promising ways of producing subfemtosecond coherent radiation in the soft-x-ray range [1,2]. HH generation is always a complex interplay between the single-atom response to a laser field often distorted by the propagation effects and the HH field propagation, which is affected by absorption and phase matching. One has to account for these factors in order to find optimized conditions for generation. When the attosecond pulse is obtained by superposition of HH, the aim of the optimization is the phase locking (synchronization) of the emitted harmonics and the maximization of the HH flux. In this case, the emitted x-ray field will achieve high intensity and temporal coherence. As shown in [2], the HH synchronization is the key to the optimization of attosecond pulse generation by superposition of HH. As a rule, the low harmonics in the plateau are temporarily shifted in emission with respect to the following ones, while harmonics in the cutoff are fully phase locked. However, in the latter case the authors of [2] found a rapid decrease of the harmonic flux. In this paper we investigate the attosecond pulse formation when the laser pulse propagates in a self-guided configuration induced in a long gas jet. We show that in these conditions, the HH that survive in propagation are specifically those in the cutoff. Unlike the HH generated in the cutoff in a short medium, in the long jet the generation optimization can be done and was experimentally achieved [3] in both space and frequency domains. We demonstrate here that these harmonics are locked in phase and that the emitted x-ray field is a train of few pulses, each having 180–220 as duration.

Systematic investigations have been conducted recently in our group in order to achieve generation optimization [3–6]. The work recently reported in [3] maximized the harmonic generation volume by inducing a profile-flattened, self-guided regime of beam propagation in a long gas jet, and achieved the generation of spectrally sharp harmonics by adding an appropriate chirp to the laser frequency. The emission volume was maximized by placing the jet about one Rayleigh length ($z_R$) before the focus, while the brightness optimum was obtained when using negatively chirped (NC) pulses. On the contrary, with positively chirped (PC) pulses, the spectra were diffuse, although the energy contained in one harmonic did not decrease too much.

Intensive numerical modeling under these particular conditions was performed in order to understand the experimental findings. The results are reported in the preceding article [7], hereafter referred to as I. We used a three-dimensional (3D) model [8] for the propagation of both the driving field and the harmonic field. Our results confirmed the formation of the self-guided configuration for the laser beam, and qualitatively reproduced the spatial and spectral distribution of the generated HH. In particular, when using NC pulses, the distribution of the harmonic field was found to be spatially and spectrally confined, being generated compactly around the propagation axis with a sharp spectral profile. The PC pulse generates a broad spectral distribution on axis, and sharper off axis, but in this case with higher spatial divergence. We found that the spatial and temporal modifications produced to the laser pulse during propagation are reflected in the single-atom response and ultimately in the HH characteristics.

Solving the wave equation for the harmonic field propagation does not reveal the mechanism of HH formation during propagation. To understand the mechanism of harmonic field buildup, a time-frequency analysis and a time-dependent phase-matching calculation have been performed. The time-frequency characteristics of the single-atom dipole, when compared to the corresponding distribution for the harmonic field, reveals the dynamics of harmonic generation and propagation. In particular, we clearly demonstrate that only specific trajectories, mainly those close to the cutoff trajectory, are enhanced in the propagation. An additional phase-matching calculation helps us to evidence the role played by different electron trajectories in the emission of HH and to reveal the dynamics of the harmonic generation near the cutoff. The time-frequency analysis combined with

 ©2005 The American Physical Society

the time-dependent phase-matching investigation shows that when the cutoff trajectory is phase matched, HH are emitted locked in phase and emission intensity is maximized. The calculations show that in this case the harmonic emission is a train of attosecond pulses, each having ~200 as in full width at half-maximum.

The paper is organized as follows. In Sec. II we briefly describe the numerical model used for calculating the fundamental and harmonic field propagation. The details of the time-dependent phase-matching calculation are also presented. The results of the modeling are shown in Sec. III. Time-frequency distributions of the harmonic field are analyzed in connection with the corresponding distributions of the single-atom response. The phase-matching distributions for the 61st harmonic (H61) are calculated at different times during harmonic emission. By corroborating these results we are able to coherently describe the harmonic generation with self-guided and chirped laser pulses. Conclusions are presented in Sec. IV.

## II. MODELING

HH generation requires the application of intense femtosecond laser pulse to a high-density gas medium that is partially ionized during interaction. A certain degree of medium ionization is always present and is indeed necessary for HH generation. However, besides being a fundamental ingredient for HH generation, ionization also poses serious limits by altering the applied laser field. Theoretically, there are three distinct aspects of the generation process: (i) propagation of the driving field through the ionized medium, (ii) single-atom radiation in which HH are generated and, (iii) propagation of the HH through the medium. Any realistic modeling of HH generation should give equal consideration to these three aspects. Propagation through the medium induces spatial, temporal, and spectral modifications to the original laser field, and the single-atom response will be directly affected by these modifications. Finally, harmonic field propagation must be considered because of absorption and phase-matching effects.

The 3D model used by us was proposed in [9], reviewed in I, and described in detail in [10], so that we recall here only the main features. The evolution of the laser pulse in the ionizing medium is calculated by numerically solving the wave equation Eq. (1) of I, for $E_1(r,z,t)$, the axially symmetric transverse electric field of frequency $\omega_0$. The effective refractive index $\eta$ of the medium includes dispersion, absorption, electron plasma, and nonlinear Kerr contribution. The free electron concentration was calculated using the Amosov-Delone-Krainov formula [11]. We recall that, to set the initial conditions for the differential equation we used the *measured* energy of the pulse, assuming a Gaussian beam in space and time with *measured* beam waist and pulse duration.

For the single-atom response, we used the strong-field approximation (SFA) developed analytically by Lewenstein and co-workers [13], as it proved to be able to model our experimental data. Solving the Schrödinger equation [12] at each grid point of the interaction region could improve the quality of the modeling but limits the number of runs as it is much more time consuming.

Having obtained the single-atom response, we numerically solved the wave equation for the harmonic field $E_h(r,z,t)$ [see Eq. (2) in I]. In a typical calculation the fundamental and harmonic field is defined in 256 points per optical cycle, the number of optical cycles depending on its duration (for example, we used 64 cycles for a 27 fs pulse). The spatial grid built over the interaction region has a 150-point uniform mesh in the axial direction and a 200-point nonuniform mesh in the radial direction. The nonuniform mesh solves the problem of rapid variations of the solution at the periphery of the interaction region and allows considering wide integration volumes in order to avoid reflections from its boundaries.

Detailed time-frequency dependence of the harmonic field on the atomic dipole were analyzed by using the short-time Fourier transform (STFT) [14], which yields the frequency content of a signal locally in time. It can be written as

$$S(t,\omega) = \frac{1}{2\pi}\int_{-\infty}^{+\infty} s(t')g(t'-t)e^{-i\omega t'}dt', \tag{1}$$

where $s(t)$ is the time signal under inspection. The window function $g(t)$ is sliding along the signal $s(t)$ and for each shift $g(t-t')$ we compute the usual Fourier transform of the product function $s(t')g(t-t')$. The square of the above distribution (energy density spectrum) is called a spectrogram [14] and was calculated for both atomic dipole and harmonic field. In the phase matching calculations, STFT distribution was used to obtain the instantaneous frequency of the driving field as

$$\omega(t) = \frac{\int S(t,\omega)\omega d\omega}{\int S(t,\omega)d\omega}. \tag{2}$$

As the self-phase modulation (SPM) is nonuniform over the interaction region, the phase-matching analysis must account for time-dependent phase of the $E_1(t)$ driving field. The time-independent analysis, as originally proposed by Balcou *et al.* [15], does not account for variations in time of the field phase as it assumes that this variation is uniform everywhere in the interaction region. We extended their method [15] to include the time-dependent phase, which arises due to the initial chirp and SPM. For the $q$th harmonic we calculated the polarization wave vector as

$$\boldsymbol{k}_{pol} = q\,\nabla[\phi_1(r,z,t)] + \nabla[\alpha\overline{I}(r,z,t)], \tag{3}$$

where $\phi_1$ is the fundamental field phase, and $\alpha$ the phase coefficient [16] for the $q$th harmonic. This coefficient was calculated for the long and short trajectories and also for the cutoff trajectories, as will be described in Sec. III. To obtain the phase $\phi_1(r,z,t)$ of the fundamental, we assumed that the spatial and temporal parts can be estimated separately as

$$\phi_1(r,z,t) = \varphi'(r,z) + \varphi''(t). \quad (4)$$

The spatial term $\varphi'(r,z)$ is obtained from the solution $E_1(r,z,\omega)$ of the propagation equation, by using the method described in [10]. The time-dependent term, due to the chirp and SPM, can be calculated from the instantaneous frequency, as

$$\varphi''(t) = \int \omega(t')dt'. \quad (5)$$

In this calculation, we first estimated $\varphi'(r,z)$, which can be regarded as the phase at the end of the laser pulse. The time-dependent part $\varphi''(t)$ was then calculated and added over the spatial part. These two parts are not completely independent, however, they cannot be easily disentangled. Considering them additively seems not to be a bad approximation because the results of the time-dependent phase-matching analysis are in very good agreement with other results in the paper.

In Eq. (3), $\overline{I}(r,z,t)$ was calculated from the propagated solution $E_1(r,z,t)$ by averaging over one optical cycle around $t$. Following Balcou [15], we define a coherence length $L_{coh}=\pi/\delta k$ where $\delta k=2\pi q/\lambda-|\boldsymbol{k}_{pol}|$, which will be now a function of space and time coordinates. We want to stress again that $\overline{I}(r,z)$ and $\phi_1(r,z)$ are here obtained from the calculated solution of the propagation equation, *not* from the unperturbed fundamental field. The advantage of this procedure is that, as all the nongeometrical effects (dispersion, absorption, ionization) are already included in $L_{coh}$, one needs not considering them separately, as is done in general.

## III. RESULTS AND DISCUSSION

### A. Time-frequency analysis

The propagation of the laser pulse was modeled using parameters that mimic our optimized experimental conditions as closely as possible. As described in [3], the optimum harmonic emission was obtained by placing the long gas jet at a distance $z_0 \approx -z_R$ in the converging beam. All the results presented here refer to this position of the jet, in which a 5 mJ, 42 fs pulse propagates through a Ne gas medium of 9 mm length, and 40 Torr pressure. We performed separate calculations for PC and NC pulses, both having the same absolute chirp value $8\times10^{-4}$ fs$^{-2}$, and then analyzed the laser field, single-atom response, and harmonic field by using the short-time Fourier transform.

Propagation through the ionized gas induces temporal modification to the initial pulse, as shown in Fig. 1. For both cases modeled, the trailing part of the laser pulse interacts with the generated plasma and is shortened from 42 fs to about 30 fs, in addition to the shift in time (around five optical cycles) of the pulse peak toward the leading edge of the pulse. The ionization dynamics is modified accordingly: the ionization fraction increases to about 4% in the time range from $t=-10$ to $t=-2$ optical cycles. The effective refractive index $\eta$ follows the jump of the electron concentration, decreasing from $\eta\gtrsim1$ to $\eta<1$ due to the dominant contribution of the electron plasma over the neutral contribution and the Kerr contribution. We can thus see that the plasma-induced defocusing dominates over the effects of self-focusing and group velocity dispersion. A numerical study of the propagation of a 100 fs pulse in Ar at 1 atm pressure also reported the pulse shortening and shifting to earlier time, due mainly to plasma defocusing [17]. In addition, a very recent result [18] shows that pulse shortening can be obtained inside a hollow waveguide filled with a gas at variable pressures and ionizing intensities. Spatial effects and ionization plasma were found to be the main factors contributing to the pulse shortening. Our calculations show that both PC and NC pulses generate the same spatial distribution of the laser intensity, because the chirp has only a very small influence on the ionization dynamics. In addition, very similar pulse shortening and shifting in time were obtained for both cases.

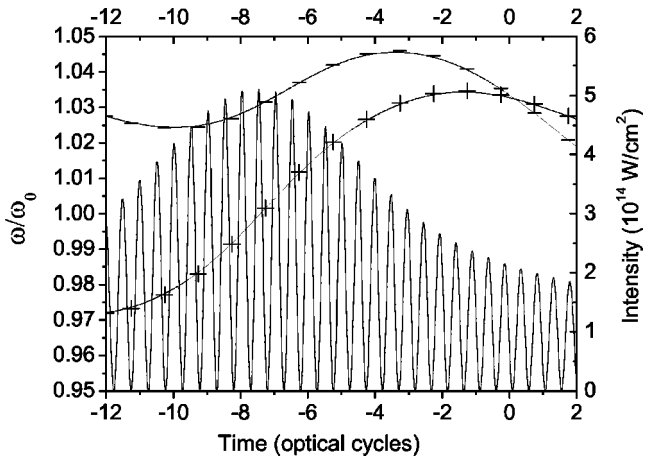


FIG. 1. Intensity (solid line) and instantaneous frequency (solid line plus symbols) of the PC (+) and NC (−) pulses at the exit of the gas jet ($z=9$ mm and $r=0$).

Due to the SPM induced in the ionizing medium, the laser frequency (see Fig. 1) increases with time (the chirp becomes positive even for the NC pulse) concomitant to the increase of the ionization fraction, and then decreases (gaining a negative chirp) back to the linear frequency variation. The way in which plasma-induced SPM affects the spectral characteristics of the NC and PC pulses lead to different conditions for the dipole emission and, subsequently, for harmonic generation. To illustrate this we first present in Fig. 2 the time frequency distribution of the single-atom response at the entrance of the interaction region. For these unperturbed pulses, every harmonic is characterized by a pattern having the shape of a $\infty$ sign (see [19] for a detailed analysis). For PC pulses the shape is well defined and one can identify the short (with smaller slope) and long (with larger slope) trajectories contributing to the nonlinear dipole. The short trajectory has a smaller slope, due to the compensation of the laser chirp by the dynamically induced chirp of the dipole. The long trajectory maintains a larger negative slope as the dynamic chirp is dominant over the pulse chirp, due to the longer excursion time of the electron. For NC pulses the shape is very much stretched in frequency. Both trajectories have large negative slopes, as in both cases the dynamic and the applied chirps sum up. We see here the power of the time-frequency analysis: a simple time or frequency dependence of the single-atom response cannot give clear informa-

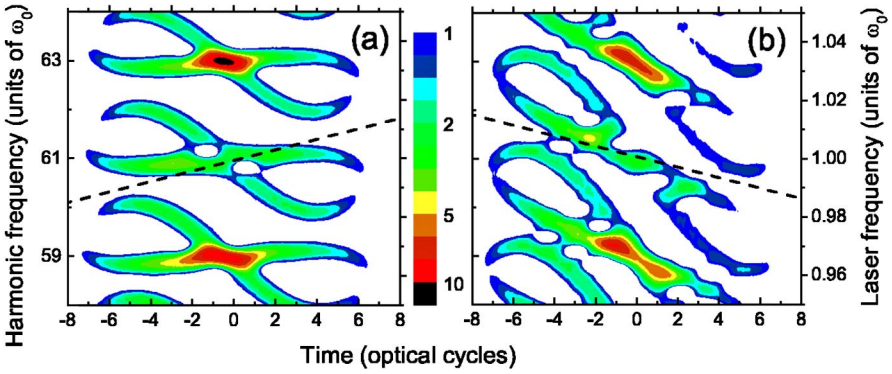


FIG. 2. (Color online) Spectrograms of the atomic dipole (logarithmic scale blue:red=1:10), as generated by the unperturbed PC (a) and NC (b) pulse at $z=0$ mm and $r=0$. The instantaneous frequency of the corresponding laser fields is also shown by the dashed line.

tion on generation dynamics, especially for the NC case.

In contrast to the results plotted in Fig. 2, the time-frequency distribution of the dipole generated after 9 mm of propagation are very different. In Fig. 3 we have plotted, for both the PC (a) and NC (b) pulse, the time-frequency distribution of the atomic dipole as it develops at $z=9$ mm and $r=0$. One can see the shift towards earlier times and shortening in time, following the driving field plotted in Fig. 1. In both cases the dipole radiates mainly in the range from $t=-10$ to $t=-2$ optical cycles, that is, in the rising ionization front, when both pulses have a positive chirp. The value of this chirp will determine the time-frequency distribution of the dipole. Indeed, in this time range the chirp is 2–4 times higher for the PC pulse compared to the NC pulse. As a result, the single-atom response is weaker in intensity and broader in frequency for the PC pulse, while for the NC pulse the distribution is more confined in frequency, and has a stronger intensity. Despite the distortion of the time-frequency distribution, we can still identify the short and long trajectories in Fig. 3, if we take into account the fact that the short trajectory has a smaller intrinsic chirp, thus, its time variation almost follows the time dependence of the instantaneous laser frequency. We confirmed this was correct by recalculating the dipole with the contributions only from short trajectories, excluding the contributions from the long trajectories.

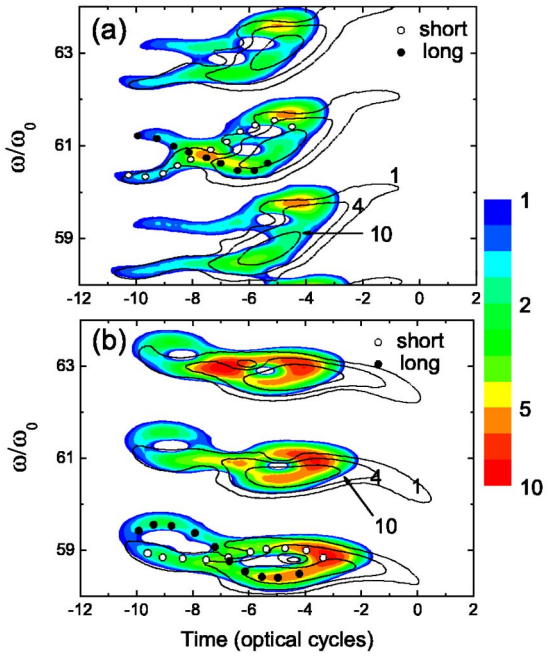


FIG. 3. (Color online) Spectrograms of the atomic dipole (logarithmic scale blue:red=1:10) and harmonic field (contour plot, logarithmic scale 1:10) at $r=0$ and $z=9$ mm, as generated by the PC (a) and NC (b) pulse. Black/white dots help tracing of the long/short trajectories.

We solved the wave equation for the harmonic field, and obtained $E_h(r,z)$, defined in the grid points over the interaction region. Shown in Fig. 3 are the time-frequency distributions of $E_h$ at $z=9$ mm and $r=0$, for PC (a) and NC (b) cases, respectively. The harmonic field and dipole distributions do not completely overlap, which shows beautifully the selection of specific trajectories as a result of harmonic field propagation. Some trajectories are enhanced even at low-intensity dipole radiation; other trajectories, although strongly present in the single-atom response, do not survive in the propagation. Both fields have a maximum intensity distributed mainly at the confluence between the long and the short trajectories, around $t=-4$ for NC and $t=-5$ for PC pulse. We note that the maximum H61 field is born at low-intensity dipole radiation, at the minimum necessary laser intensity to generate the single dipole for H61; this clearly indicates the generation in the cutoff regime.

It is well known that for a harmonic in the plateau, there are (within one optical cycle) two trajectories that yield the same kinetic energy, and which therefore contribute to the same harmonic [see the inset of Fig. 7(a)]. With increasing harmonic order, thus approaching the cutoff, the two trajectories become closer and, for the maximum achievable kinetic energy, they coincide. As shown in [20], the two trajectories do not contribute equally to the total emission; moreover; there are more trajectories (with larger excursion times) that become important, especially for the harmonics in the plateau. These trajectories are not included in our modeling, as the integration time for the dipole moment was only 1.2 optical cycles. This is reasonable because the harmonics in study are very close to the cutoff.

Bearing in mind the above consideration, we can now analyze the data in Fig. 3. One can see that the final harmonic field is built up from the contributions of both short and long trajectories. However, in the NC case, the harmonic field builds up mainly on the short trajectory pattern of the single-atom response, despite the fact that SFA tends to overestimate [20] the long trajectory contribution. The result is a

frequency profile even narrower than that of the corresponding single dipole. The emission spans in time over 10 optical cycles, but in a narrow frequency range, which generates a high spectral brightness. In the case of PC pulse, harmonics are also built from both short and long trajectories; however, the final field spans over two harmonic orders in frequency, which practically means overlapping between two adjacent orders, in full agreement with the experimental findings [3].

Using the instantaneous frequency data we can estimate the average blueshift of the fundamental field for the time interval corresponding to the atomic dipole emission; namely, from about $t=-10$ to $t=-2$ optical cycles. We obtain on average $1.5\%\omega_0$ and $3.1\%\omega_0$ for NC and PC pulses, respectively. Comparing these values with the spectral spread of the atomic dipole ($0.9\omega_0$ and $1.9\omega_0$, respectively), we conclude that the chirp of the driving laser pulse is transferred to the $q$th component of the dipole as $q$ times the fundamental chirp. However, the driving field chirp is *not* directly transferred to the $q$th harmonic, contrary to what was reported recently [21,22]. As we see from Fig. 3, this is because in a long target the phase matching plays a very selective role in the HH generation process, by eliminating some trajectories and enhancing others. In [21], the observation of sharp harmonic peaks for relatively low-intensity PC pulses support the assumption of dominant single-atom effects, in agreement with the transfer of $q$ times the chirp from the driving field to the $q$th harmonic, which was also observed.

We can conclude that the time-frequency analysis shows the tight causal connections between the driving field and the single-atom dipole, and between the latter and the harmonic field characteristics. The dipole radiates in a very restricted time range during laser pulse; namely, during the rising ionization front. This was shown to be specific for the cutoff HH [23]. We also demonstrated that the harmonic field is formed by selecting specific trajectories at specific time moments from the dipole response. For the understanding of this trajectory selection, a phase-matching analysis was proved to be necessary.

### B. Phase-matching analysis

The initial chirp of the driving field combined with the plasma-induced SPM plays an important role in determining the single-atom response; thus, one must also account for these effects in the phase-matching analysis. A first benefit of such an analysis would be to determine the way they influence the final harmonic field: whether the consideration of only the single-atom response is enough to explain the harmonic output or whether the phase-matching process should be considered as well. Second, from the analysis we would be able to determine the relative importance of these two factors and their specific action in building the harmonic field.

The dipole emission for a given harmonic, as shown in Fig. 3, takes place in a very limited time interval during the pulse evolution. The condition of the laser field during this time interval, such as its amplitude and phase, directly influences atomic dipole amplitude and phase. However, we have seen in the preceding section that only specific dipole phase components are enhanced by the propagation and give the final harmonic field. Therefore, one must analyze the phase-matching condition over the time range where dipole emission is significant. We should point out that the time-dependent phase matching calculation proved to be essential for the analysis of harmonic field generation.

The phase-matching status of HH generation can be well represented by the coherence length $L_{coh}$. The calculation of $L_{coh}$ for different trajectories is as follows. We calculate the time-frequency distribution of the dipole generated by a *chirpfree* 42 fs pulse, and identify the short and long trajectories. From these calculations we derived $\alpha_s=4$ and $\alpha_l=22\times10^{14}$ cm$^2$/W for the short and long trajectories, respectively. These values are well known and agree well with similar calculations [19]. In the cutoff region we assumed that the dipole phase $\Phi$ can still be approximated by the linear relation $\Phi=-\alpha I$ and, using $\delta\omega=\partial\Phi/\partial t=-\alpha\partial I/\partial t$, we estimated a value $\alpha_c=13\times10^{14}$ cm$^2$/W, for the trajectories close to the cutoff one. These values were used in phase-matching calculations, as will be shown further on. However, we should keep in mind that this value of $\alpha_c$ is not a constant, but depends on the laser intensity and harmonic order, and hence it can only be used in a limited range of laser intensities ($\sim3.5\times10^{14}$ W/cm$^2$ in our case).

We calculated $L_{coh}$ distributions for different time instants in the range from $t=-10$ to $t=+2$ optical cycles. This is the time measured in the moving frame and referenced to the center of the unperturbed laser pulse. Plotted in Figs. 4–6 are the values of $L_{coh}$ for the short, long, and cutoff trajectories, respectively, and from $t=-6$ to $t=-1$ optical cycles. For $t<-6$ we did not observe significant changes in the $L_{coh}$ map, while for $z=9$ mm and $t>-1$ the laser intensity is below the cutoff intensity for H61. In general, the obtained $L_{coh}$ maps are similar for the PC and NC pulses, in all three cases. Nevertheless, the differences can be singled out and assigned to specific characteristics of the harmonic field. The calculation in Figs. 4–6 was performed for a 15 mm long jet; however, we have to keep in mind that we are interested in only the first 9 mm of propagation.

The short trajectory in Fig. 4 develops a good on-axis phase matching for $t$ ranging from $-5$ to $-1$, with maximum of $L_{coh}$ at $t=-1$. For $t>-1$, $L_{coh}$ is increasing on axis; however, the case is of no further interest because of low laser intensity. The $L_{coh}$ maximum is between $z=6$ mm and $z=9$ mm, so that this good phase matching will give an on-axis contribution to the harmonic field. The coherence length is clearly higher for NC pulses, which indicates that short trajectories are better phase matched with NC pulses. The off-axis region of good phase matching, developing at $r\approx60$ $\mu$m, probably does not count as it is developed for $z>9$ mm for most of the time interval considered.

For the long trajectory case in Fig. 5, the differences between the PC and NC cases are larger, and $L_{coh}$ have larger values for the PC case. The PC pulse develops a good off-axis phase matching in the interval from $t=-5$ to $t=-2$, for $r$ around 20–25 $\mu$m and for $z$ between 3 and 9 mm. The NC pulse has the best phase matching conditions, still rather poor only for $t=-4$, and in a restricted space region around $z=7$ mm. The clearly larger $L_{coh}$ obtained for PC pulses is an indication that long trajectories are better phase matched with PC pulses.

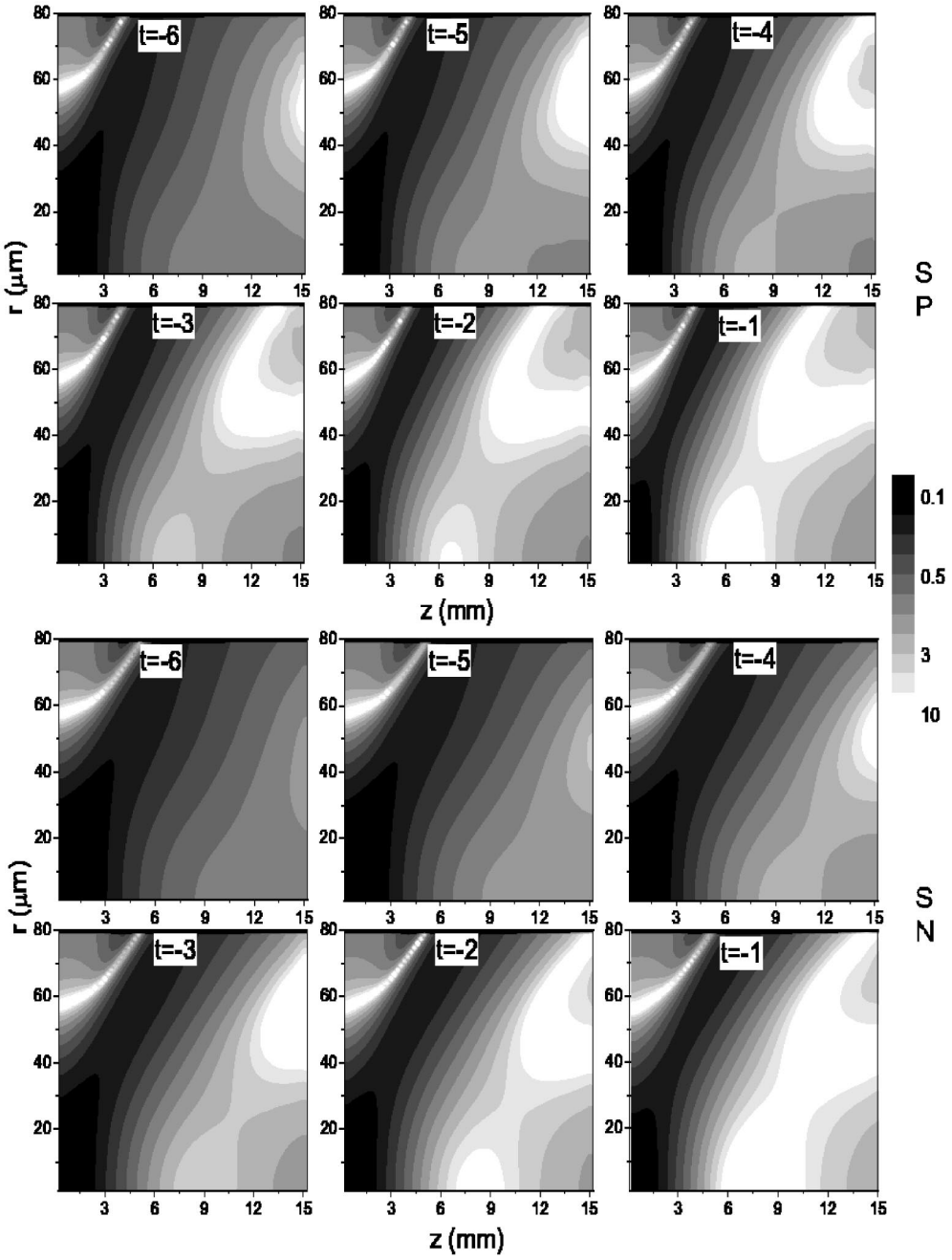


FIG. 4. Coherence length distributions for H61, corresponding to the short (S) trajectory, for positively (P) and negatively (N) chirped pulses. Time in optical cycles is referred to the unperturbed laser pulse peak.

However, the analysis of the phase matching created by the two trajectories, either short or long, is only indicative for the characterization of the generation process in our case. As we can see from Fig. 3, the main harmonic field develops at the confluence between the short and long trajectories. In fact, all trajectories surviving in the propagation are close (in terms of birth and recollision moment of the electron) to the cutoff one. The calculated $L_{coh}$ for cutoff trajectories is plotted in Fig. 6. First, one must note that in this case the differences between the maps generated with PC and NC pulses are still observable, but are smaller than the differences obtained for long and short trajectories. If we start our analysis from the PC case in Fig. 6, we find that there is a good on-axis phase matching starting at $t=-5$ around $z=9$ mm. At $t=-4$ the maximum of $L_{coh}$ is clearly localized between 6 and 9 mm for both PC and NC case. Further on, at $t=-3$, HH are generated under the phase-matching condition, because $L_{coh}$ is higher than the propagation length. This takes place for both PC and NC pulse, between 5 and 9 mm and for a region extending radially up to 40 $\mu$m. For $t=-2$ and $t=-1$ the good phase matching is maintained, but only off axis around 30 $\mu$m, with a slightly larger $L_{coh}$ for the PC pulse.

At this point we should recall that, solving the propagation equation for the harmonic field, we obtained in I the radial and spectral distribution of the harmonic field after $z=9$ mm of propagation. In particular, when using NC pulses,

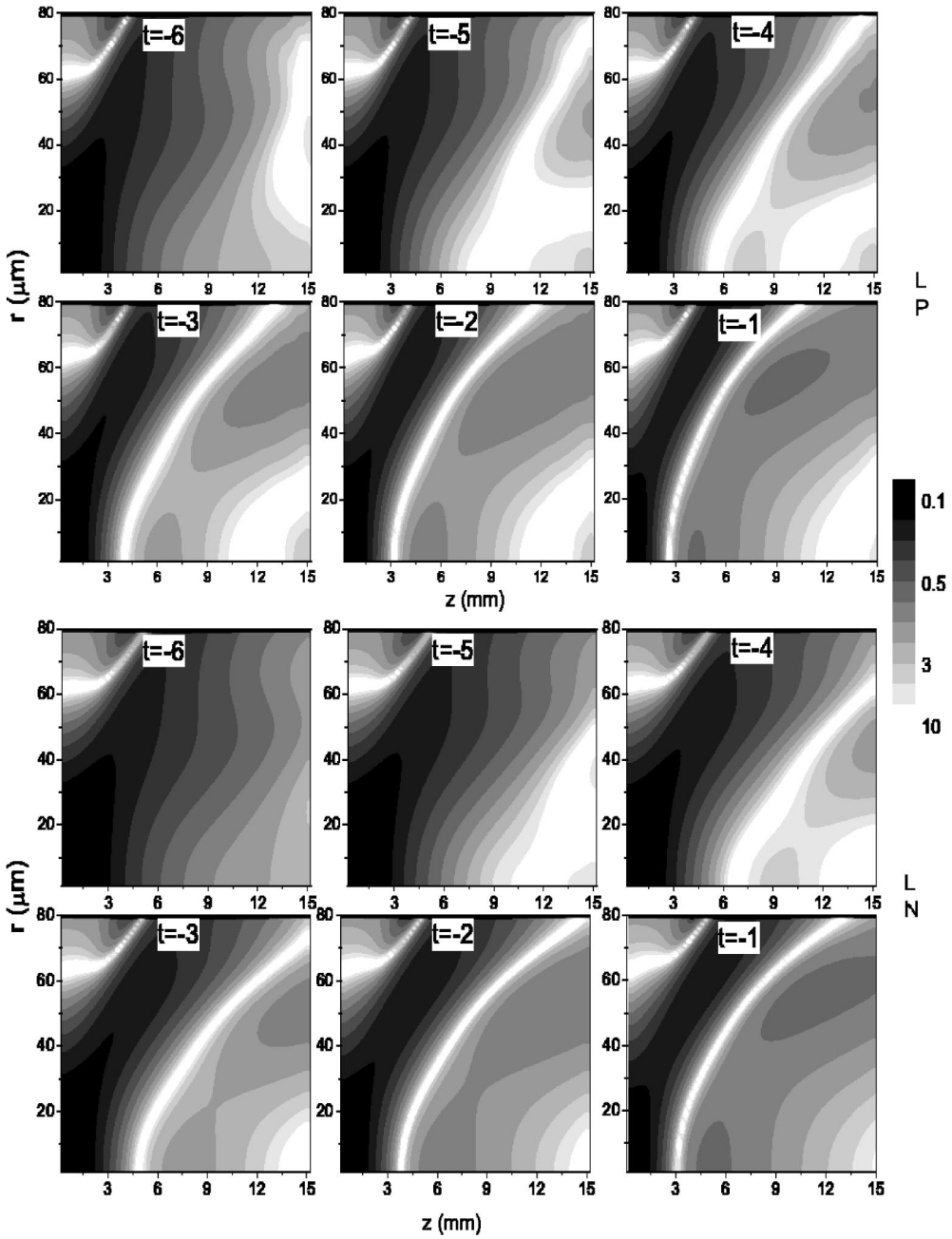


FIG. 5. Coherence length distributions for H61, corresponding to the long (L) trajectory, for positively (P) and negatively (N) chirped pulses.

each harmonic around H61 was generated as spectrally sharp and spatially compact around the propagation axis. An initial positive chirp in the fundamental pulse generates a broad spectral distribution on axis, and sharper off axis. We are now in a position to assume that the good phase-matching event, taking place from $t=-5$ to $t=-3$, is responsible for the good emission close to the propagation axis, which was observed in experiment [3] and reproduced in modeling reported in I for both PC and NC pulses. Experimentally, we found that the energy contained in one harmonic was comparable for both pulses. The chirp of the PC and NC pulses, within this range of time, produces the difference in spectral distributions. We can see from Fig. 1 that for the NC pulse the chirp is positive but small, vanishing around $t=-3$, while the PC pulse still has a large positive chirp. The PC pulse yields a narrow spectral width field at off axis, as seen in I. This narrow spectral width is the combined effect of two causes: the off-axis generation (where the SPM is smaller than on axis) and the later generation in time (at $t>-2$ where the positive chirp is decreasing).

We also see from Fig. 3 that the harmonic field extends at later times, notwithstanding that the corresponding dipole is extremely weak. This is due to the very good phase matching of the short trajectory (see Fig. 4) for $t>-1$, which adds constructively the $z<9$ mm contributions of the single dipole. The time-frequency distribution of these contributions

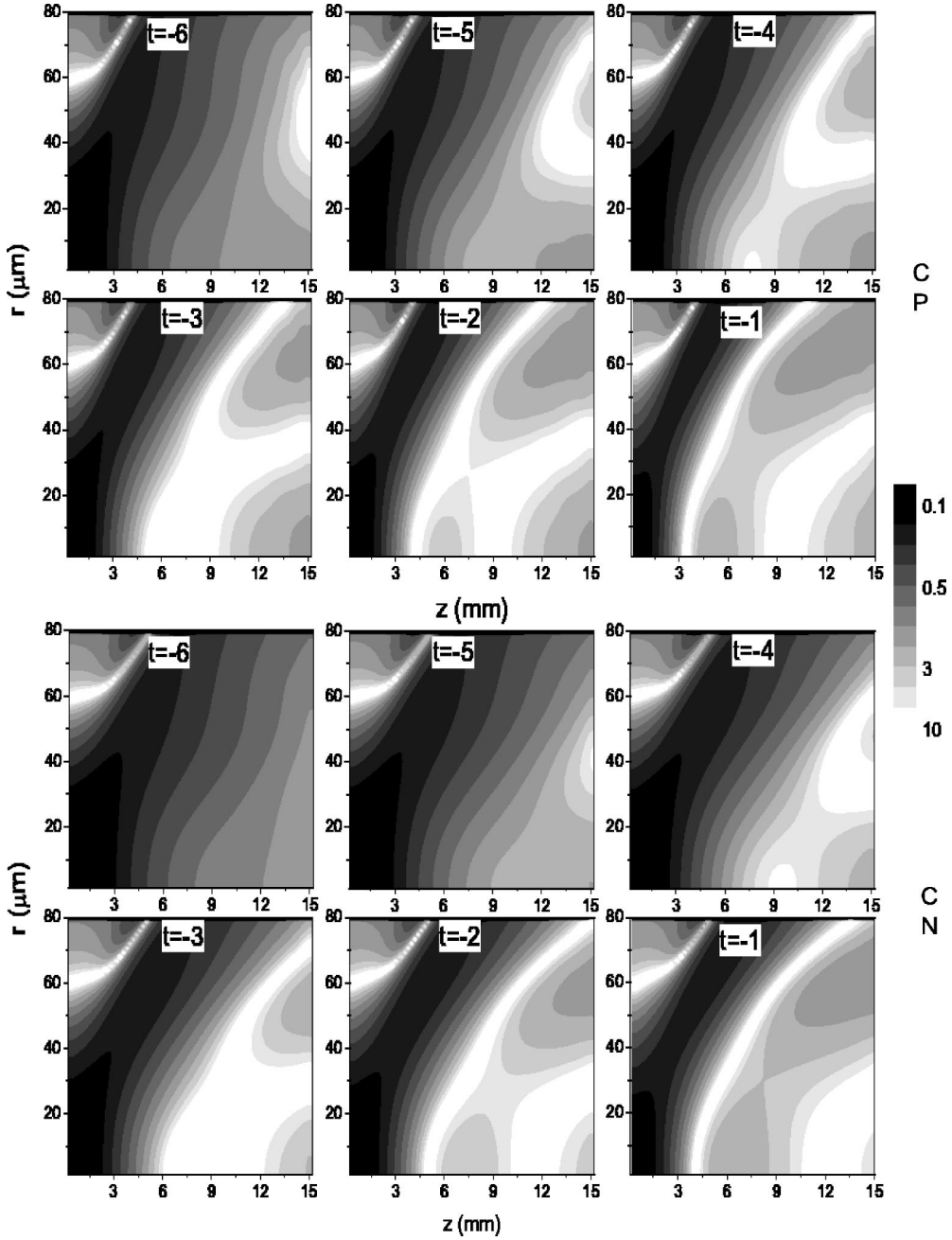


FIG. 6. Coherence length distributions for H61 corresponding to the cutoff (C) trajectory, for positively (P) and negatively (N) chirped pulses.

shows that, with decreasing $z$, they are more extended and less shifted in time, giving a sizable contribution for $t>-1$.

### C. Harmonic synchronization in the cutoff

The time-frequency distribution in Fig. 3 reveals the frequency details of the harmonic field, and for this purpose we used a large temporal window (4 optical cycles). To see the details in time domain we recalculated the distribution with a narrow (0.125 optical cycles) time window. The frequency resolution is lost, but the temporal resolution relevant for the harmonic emission is recovered. Doing this for every harmonic $q$, i.e., calculating the STFT distribution of the field $E_h(r=0,z=9,\omega)$ for $(q-1)\omega_0<\omega<(q+1)\omega_0$, we obtained the necessary time resolution so as to estimate the moment of maximal emission for every harmonic, at each half optical cycle. The results are given in Fig. 7 for the NC pulse, and for the HH between H55 and H65, which are the most intense in both the calculated and the experimental spectra [3]. We obtained similar results for the PC pulse. The locking in time is slightly better and the total harmonic pulse is narrower in time, in agreement with the spectrally broad HH observed in this case [3].

The reading of these results can be easily done if we have in mind the electron classical dynamics during the HH generation process [see the inset of Fig. 7(a)]. During each op-

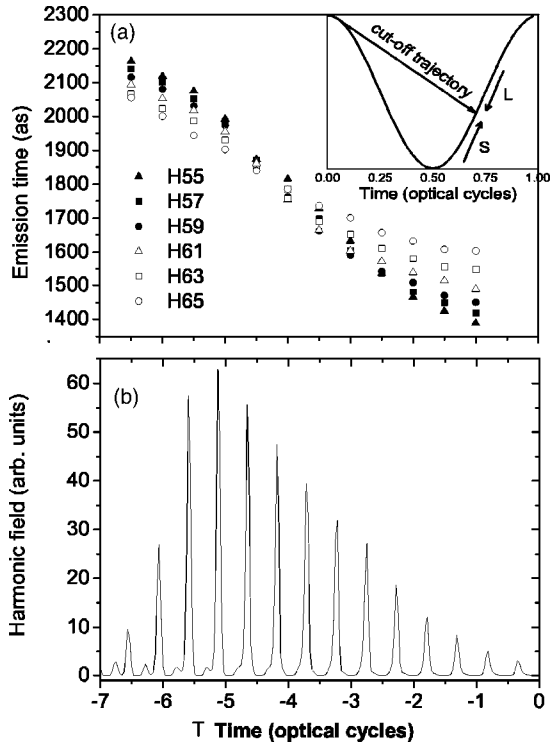


FIG. 7. (a) Emission time of the harmonics from H55 to H65 for the NC pulse. The inset shows the cutoff electron trajectory in a frame oscillating at the field frequency (Kramers Henneberger frame) in which the electron moves in straight lines. The two arrows show the direction of increasing harmonic order along the short (S) and long (L) trajectories. (b) The sum of the STFT modulus of the same harmonics.

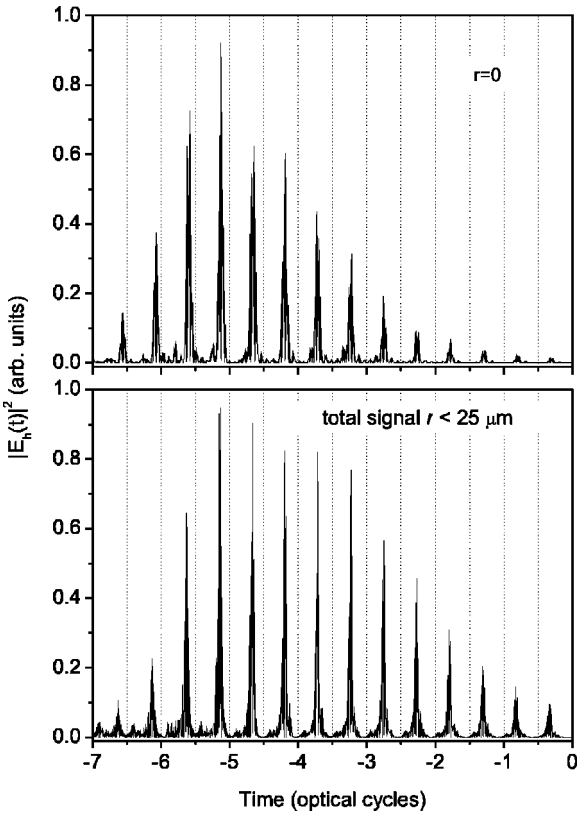


FIG. 8. Time dependence of the harmonic field, for the NC pulse, at the exit from the interaction region, for $r=0$ (a) and integrated up to $r=25$ $\mu$m (b). It was calculated as the inverse Fourier transform of $E_h(\omega)$, where $54\omega_0<\omega<66\omega_0$.

tical half-cycle, a harmonic can be emitted two times, namely, when the short or long trajectory closes and electron recombines with the parent atom. The two recombination moments become closer to each other as the harmonic order increases and approaches the cutoff order. In other words, along the short trajectory, the later the recombination moment, the higher the kinetic energy gained, thus, higher harmonics are created later. Long trajectories generate higher harmonics when electron recombines at earlier time, thus, higher harmonics are created sooner. This enables us to precisely describe the generation dynamics during pulse evolution. Analyzing the earlier interval of emission (laser cycles with $t<-5.5$), we observed that higher harmonics are generated before lower harmonics, thus they are generated from long paths. This is in agreement with the phase-matching map in Fig. 5, which indicates a good phase matching for long trajectories at earlier times. The harmonics from H55 to H65 are almost fully locked in time for the time range around −5.5, which is also close to the maximum emission intensity. For later times, the emission order for the HH is reversed: lower harmonics are generated first, which means that the harmonics are generated along the short path, but with lower intensity. This is again in agreement with the phase-matching maps, as for the cutoff paths the good phase matching is evidenced in Fig. 6 for $-5<t<-2$, while for the short paths $L_{coh}$ in Fig. 4 is increasing for later times.

The sum of time-frequency distributions of the harmonics from H55 to H65, plotted in Fig. 7(b), show that the total emission field is a train of attosecond pulses. These data, correlated to that in Fig. 6, demonstrate that the HH around H61 are generated mainly from cutoff trajectories, which provide the maximum contribution to the emission intensities. Long trajectories have a sizable contribution at earlier times, while short trajectories have a smaller contribution. The long trajectories have the phase matching correlated in time with the maximum of the laser intensity, both taking place at $t\simeq-5$, which explains their larger contribution to the total emission. At later times, when the short trajectories have their best phase matching, the laser intensity is decreased to values which are below the cutoff value for H61, which means a smaller contribution to the emission.

The total intensity of $E_h(r,z=9,t)$ for the NC case, obtained through an inverse Fourier transform of the solution $E_h(r,z=9,\omega)$, is shown in Fig. 8 for $r=0$ (a) and integrated from $r=0$ to $r=25$ $\mu$m (b). The $r=0$ data are similar to that in Fig. 7, and the emitted attosecond pulses at $r=0$ are well synchronized to the corresponding pulses of the integrated field. Good synchronization in the radial direction is a consequence of homogeneous generation conditions that exist in the self-guided region for the NC pulse. For the same reason, in this $r$ range, H61 is emitted with almost the same intensity, as is shown in Fig. 7 of I. The maximum harmonic field at $r=0$ is emitted at $t=-5$, but for $r>0$, this maximum shifts towards later times, due to the corresponding shift of the driving field. This shift changes the intensity distribution of

the pulses in Fig. 8(b), enhancing the pulse intensities at later times. From the data in Fig. 8(b), we can estimate the duration of the emitted attosecond pulses, as ranging from 180 to 225 as. The duration of the total signal, including contributions from larger $r$ will be probably longer, however, the good synchronization will keep the attosecond pulse duration within the same range.

## IV. CONCLUSIONS

We presented an analysis of HH generation when chirped pulses are propagated in a self-guided configuration through a long gas jet. The time-frequency distributions of the single-atom response and of the harmonic field demonstrate that only the cutoff trajectories survive to build up the final harmonic field. A time-dependent phase-matching calculation, taking into account the chirp and self-phase modulation of the driving field, was performed. Phase-matching distributions for different time instants during dipole emission were obtained. For the cutoff trajectories, phase-matched HH are generated by only a few optical cycles during single-atom emission.

In a self-guided configuration the harmonic generation is accompanied by an appreciable degree of ionization, which affects the process in several ways. However, the decrease of the initial laser intensity can be controlled to some extent by selecting the atom, or by adjusting the pulse duration and/or pressure. The generation volume can be controlled and maximized by changing the jet position with respect to the focus, as was experimentally demonstrated [3]. We found that a small number of harmonics, those which have the single atom response in the plateau but close to the cutoff, prove to have favorable phase-matching conditions, and are finally generated from cutoff trajectories, with high spectral brightness (by adjusting the initial chirp) and good temporal phase locking.

## ACKNOWLEDGMENT

The research was supported by the Korea Science and Engineering Foundation (KOSEF) through the Creative Research Initiative Program.

[1] M. Lewenstein, Science **297**, 1131 (2002).
[2] Y. Mairesse, A. de Bohan, L. J. Frasinski, H. Merdji, L. C. Dinu, P. Monchicourt, P. Breger, M. Kovacev, T. Auguste, B. Carre, H. G. Muller, P. Agostini, and P. Salieres, Phys. Rev. Lett. **93**, 163901 (2004).
[3] H. T. Kim, I. J. Kim, D. G. Lee, K. H. Hong, Y. S. Lee, V. Tosa, and C. H. Nam, Phys. Rev. A **69**, 031805(R) (2004).
[4] H. T. Kim, D. G. Lee, K.-H. Hong, J.-H. Kim, I. W. Choi, and C. H. Nam, Phys. Rev. A **67**, 051801(R) (2003); H. J. Shin, D. G. Lee, Y. H. Cha, K. H. Hong, and C. H. Nam, Phys. Rev. Lett. **83**, 2544 (1999).
[5] D. G. Lee, H. J. Shin, Y. H. Cha, K. H. Hong, J.-H. Kim, and C. H. Nam, Phys. Rev. A **63**, 021801(R) (2001).
[6] D. G. Lee, J.-H. Kim, K.-H. Hong, and C. H. Nam, Phys. Rev. Lett. **87**, 243902 (2001).
[7] V. Tosa, H. T. Kim, I. J. Kim, and C. H. Nam, preceding paper, Phys. Rev. A **71**, 063807 (2005).
[8] V. Tosa, E. Takahashi, Y. Nabekawa, and K. Midorikawa, Phys. Rev. A **67**, 063817 (2003).
[9] E. Priori, G. Cerullo, M. Nisoli, S. Stagira, S. De Silvestri, P. Villoresi, L. Poletto, P. Ceccherini, C. Altucci, R. Bruzzese, and C. de Lisio, Phys. Rev. A **61**, 063801 (2000).
[10] E. Takahashi, V. Tosa, Y. Nabekawa, and K. Midorikawa, Phys. Rev. A **68**, 023808 (2004).
[11] M. V. Amosov, N. B. Delone, and V. P. Krainov, Zh. Eksp. Teor. Fiz. **91**, 2008 (1986).
[12] J. L. Krause, K. J. Schafer, and K. C. Kulander, Phys. Rev. A **45**, 4998 (1992); I. P. Christov, M. M. Murnane, and H. C. Kapteyn, Phys. Rev. Lett. **78**, 1251 (1997).
[13] M. Lewenstein, Ph. Balcou, M. Yu. Ivanov, A. L'Huillier, and P. B. Corkum, Phys. Rev. A **49**, 2117 (1994).
[14] L. Cohen, *Time Frequency Analysis* (Prentice Hall, Englewood Cliffs, N.J., 1994).
[15] P. Balcou, P. Salières, A. L'Huillier, and M. Lewenstein, Phys. Rev. A **55**, 3204 (1997).
[16] M. Lewenstein, P. Salières, and A. L'Huillier, Phys. Rev. A **52**, 4747 (1995).
[17] M. Mlejnek, E. M. Wright, and J. V. Moloney, Phys. Rev. E **58**, 4903 (1998).
[18] N. L. Wagner, E. A. Gibson, T. Popmintchev, I. P. Christov, M. M. Murnane, and H. C. Kapteyn, Phys. Rev. Lett. **93**, 173902 (2004).
[19] J. H. Kim, D. G. Lee, H. J. Shin, and C. H. Nam, Phys. Rev. A **63**, 063403 (2001).
[20] M. B. Gaarde and K. J. Schafer, Phys. Rev. A **65**, 031406(R) (2002).
[21] Z. Chang, A. Rundquist, H. Wang, I. Christov, H. C. Kapteyn, and M. M. Murnane, Phys. Rev. A **58** R30 (1998).
[22] J. Mauritsson, P. Johnsson, R. Lopez-Martens, K. Varju, W. Kornelis, J. Biegert, U. Keller, M. Gaarde, K. J. Schafer, and A. L'Huillier, Phys. Rev. A **70**, 021801(R) (2004).
[23] S. C. Rae, K. Burnett, and J. Cooper, Phys. Rev. A **50**, 3438 (1994).